Accepted Manuscript

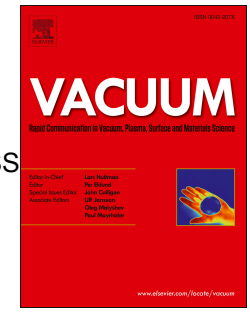

x-ray tomography study on porosity in electron beam welded dissimilar copper–304SS joints

Jyotirmaya Kar, Soumitra Kumar Dinda, Gour Gopal Roy, Sanat K. Roy, Prakash Srirangam

PII: S0042-207X(17)31489-6

DOI: 10.1016/j.vacuum.2017.12.038

Reference: VAC 7744

To appear in: *Vacuum*

Received Date: 28 October 2017

Revised Date: 22 December 2017

Accepted Date: 23 December 2017

Please cite this article as: Kar J, Dinda SK, Roy GG, Roy SK, Srirangam P, x-ray tomography study on porosity in electron beam welded dissimilar copper–304SS joints, *Vacuum* (2018), doi: 10.1016/j.vacuum.2017.12.038.

X-RAY TOMOGRAPHY STUDY ON POROSITY IN ELECTRON BEAM WELDED DISSIMILAR COPPER–304SS JOINTS

Jyotirmaya Kar [1], Soumitra Kumar Dinda [1], Gour Gopal Roy [1], Sanat K. Roy [1], Prakash Srirangam [2]

[1]Department of Metallurgical and Materials Engineering, Indian Institute of Technology Kharagpur, India, 721302

[2] WMG, University of Warwick, Coventry, CV4 7AL, UK

***Corresponding Author:** jyotirmaya007@gmail.com

ABSTRACT: Dissimilar joining of copper (C10300) to AISI–304 Stainless Steel **(SS)** sheets was performed using Electron Beam Welding **(EBW)** process. EBW was performed for two weld conditions such as with beam oscillation and without beam oscillation. X-ray Computed Tomography **(XCT)** technique was used for three-Dimensional **(3D)** visualization and quantification of porosity in the weld region. It was observed that the application of beam oscillation resulted in less porosity and the average pore size was found to be smaller as compared to without beam oscillation condition. Also, pores were found to be uniformly distributed in the weld incase of with beam oscillation as compared to without beam osicllaition condition. Further, it was observed that there exists an optimum beam oscillation diameter beyond which there is no positive effect of beam oscillation in controlling the porosity formation in the weld joint.

KEYWORDS: Electron beam welding; Beam oscillation; Stainless steel; Copper; X-ray computed tomography; Porosity

==========

1. INTRODUCTION

The ability to manufacture a product using dissimilar metals/alloys by welding greatly increases the flexibility in design and production of components for engineering applications. Copper–SS dissimilar joint is one such joint which finds applications in the field of power generation industries, heat transfer components, nuclear sector, and cryogenic sector. This type of dissimilar joint is designed to provide excellent thermal and electrical conduction imparted by copper and strength, wear and corrosion resistance imparted by SS. However,

fusion welding of copper to steel is difficult owing to their large differences in physical, chemical and thermo-mechanical properties **[1,2]**. For instance, thermal conductivity of copper is much higher than that of steel, which causes difficulties in reaching its melting temperature. Besides, Cu and Fe have limited solid solubility in each other, and they undergo phase separation during solidification. These two metals also have large differences in their melting temperatures and coefficient of thermal expansion.

Copper–SS joints have been produced by using various solid state or fusion welding processes. Solid state welding processes like diffusion welding, friction stir welding **(FSW)**, and explosive welding have been extensively used **[3-8]**. In diffusion welding of copper–SS, the interlayer material, applied temperature, and pressure, etc. have been found to influence weld quality. **Sabetghadam et al. [5]** studied diffusion welding of copper to 410SS and reported that for nickel interlayer, increase in the bonding temperature increases the formation of micro voids in the bonding zone. **Xiong et al. [6]** reported that compared to pure tin, bronze or gold, use of tin-bronze-gold composite interlayer, allowed the use of comparatively lower bonding temperature, increased grain boundary wetting and tensile strength. **Imani et al. [7]** for FSW of copper–SS joints reported that off-setting of the pin toward copper side by 30% produced defect free welds with better tensile strength. **Shanjeevi et al. 2016 [8]** reported that friction pressure is the most significant process parameter of FSW followed by pin rotational speed affecting the resultant microstructure and tensile properties of copper–SS joints. For fusion welding of copper–SS, different arc welding processes and high energy density Laser Beam Welding **(LBW)** or Electron Beam Welding **(EBW)** processes have been used. In conventional arc welding, it is reported that selection of proper filler played a crucial role on weld quality in terms of welding defects such as porosity, microcracks, lack of fusion, shrinkage, etc. **[9-12]**. **Yao et al. [13]** and **Chen et al. [14]** used an off-set laser beam towards SS side for producing copper–SS joints and reported that by varying the off-set distance, copper melting in the fusion zone could be controlled. It has been reported that small amount of copper melting was beneficial in reducing defects, while presence of large amount of copper resulted inhomogeneity in composition, enhanced residual stresses, which produced severe microcracks with inferior mechanical properties of the joints **[13-15]**. The same observation has also been reported from EBW **[16-20]**. **Magnabosco et al. [21]** for EB welded copper–SS joints reported that with increase in plate thickness (30 to 70mm), defects like microcracks and porosities and heterogeneity in microstructure increased.

It is evident from literature review that both in solid state welding and arc welding of copper–SS, use of appropriate interlayer/filler metal is likely to produce better quality joints possibly by limiting the formation of deleterious intermetallics formation in the weld joint. From the study of high energy density welding, it was evident that amount of copper melting was important because an optimum amount of copper only produced a sound joint. In case of copper-steel welding, copper melting was reported to be controlled by off-setting the beam on the steel side **[13,14,19-21]**.

Copper contains dissolved gases and during solidification it produces porosities; the amount, size and distribution of which depends on copper distribution in the fusion zone. Besides, large difference in thermal conductivity and thermal expansion coefficient between copper and iron also generates strains and cracks and the severity of which might depend on copper distribution. In addition to beam off-setting, beam oscillation is also an important tool to achieve optimum melting of copper in case of high energy density welding. In addition beam oscillation by virtue of its churning action, can also mix the copper more uniformly in the weld zone. Some literature has also provided information regarding the use of beam oscillation in electron beam welding of dissimilar metal and alloys. **Wang et al. [22]** for SiCp/101Al composite joints and **Dinda et al. [23]** for steel to Fe–Al alloy dissimilar joints reported that the oscillating beam joints contained much lower porosity in the fusion zone than that produced by their non-oscillating beam counterparts. **Kraetzsch et al. [24]** reported that crack free joints of copper–aluminium dissimilar metals could be produced under a properly optimized oscillating laser beam. **Fu et al. [25]** performed EBW of Ti6.5Al2Zr1Mo1V alloy and reported that beam oscillation improved weld morphology, reduced porosity content with improved fatigue life of the joint equivalent to that of the base alloy. **Wang et al. [26]** studied the effect of various beam oscillation patterns such as transverse, longitudinal and circular in dissimilar joining of AA6061–T6 aluminium alloys and reported that the application of circular beam oscillation pattern was effective in reducing defects and producing smooth weld surface with fine equiaxed grain structure compared to other oscillation patterns.

Understanding the effect of beam oscillation on porosity formation in dissimilar joints is essential in understanding the weld quality and to improve the mechanical properties of the welds. X-ray Computed Tomography **(XCT)** technique is a powerful technique for 3D visualization and quantification of defects in the weld joints **[27-29]**. Furthermore, unlike the conventional defect analysis techniques such as X-ray radiography, ultrasonic test or dye

penetrant test, XCT enables to visualize micro pores and their location in three dimensional space in the weld joint. Further, it was observed that there were hardly any published reports on the defect analysis of copper–SS joints produced by EBW using XCT technique. This forms the scope of the present work and the objective is to characterize porosity formation using XCT analysis in electron beam butt welded copper–SS joints produced by with and without beam oscillation.

2. EXPERIMENTAL PROCEDURES

2.1. Materials

AISI–304 SS and extra low phosphorous copper (C10300) sheets having thickness of 3mm were used as base metals for this study. **Table–1** provides the chemical composition of both base metals obtained using X-ray fluorescence spectroscopy (Bruker® model: S8 TIGER). For joining, coupons having dimensions 150×80×3mm^3(welding length × breadth × thickness) were cut from the obtained metal sheets, where welding length was transverse to the rolling direction. The joining side face of each coupon was then machined followed by mechanical polishing on 240grit emery paper. Surface polishing was necessary as rough surface helps confinement of gas pockets between the two joining plates, which later leads to porosity in the joint **[30,31]**. Prior to joining, the coupons were first degreased followed by thorough cleaning with acetone.

Table–1: Chemical composition of 304 SS and copper (C10300) in weight percentage

AISI–	**Cr**	**Ni**	**Mn**	**Mo**	**Co**	**Si**	**C**	**Al**	**P**	**Fe**
304SS	18.06	8.06	1.802	0.15	0.16	0.36	0.043	0.06	0.042	Rest
Copper	**Cu**	**Pb**	**P**	**Fe**	**H**	**O**	**Ni**	**Total impurities**		
C10300	99.97	0.0001	0.003	0.001	0.008	0.003	0.003	0.03 % Max.		

2.2. Welding Procedure

The prepared coupons were subsequently butt welded in an 80kV, 12kW EBW machine **(Fig. 1)** at Indian Institute of Technology Kharagpur, India which was indigenously designed and fabricated by the Bhabha Atomic Research Center, India. In this study, total three joints were prepared, out of which, joint–1 was made with a non-oscillating beam, while joint–2 and 3 were made with an oscillating beam having oscillation frequency of 600Hz and oscillation diameters of 1 and 2mm, respectively. Since copper conducts heat

faster, prolonged dwelling of beam on copper side favors dissipation of more heat by conduction. As beam voltage (60kV) and welding velocity (1000mm/min) were maintained constant, the heat requirement was compensated by increasing the beam current and accordingly, 65mA, 73mA, and 80mA of beam currents were used for joint–1, joint–2, and joint–3, respectively.

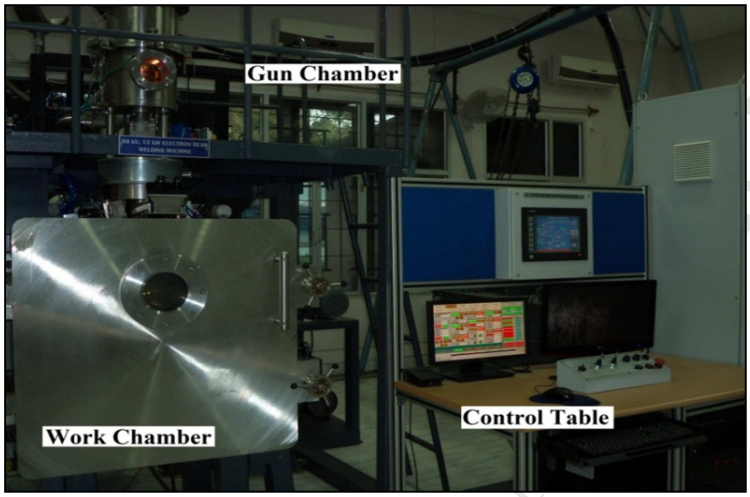

Fig. 1: 80 kV, 12 kW Electron Beam Welding **(EBW)** machine at IIT Kharagpur

2.3. Characterization Technique

After preparation, the joints were first inspected visually followed by X-ray radiography for quality check and all were found to pass the test. **Figure 2** shows the X-ray radiographic images of three dissimilar copper–SS joints.

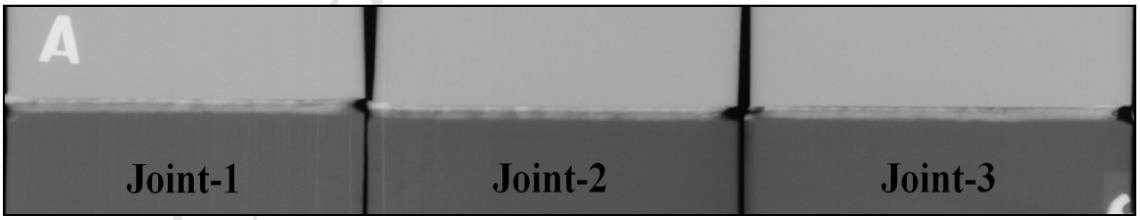

Fig. 2: X-ray radiographic images of the three prepared copper–SS joints

For 3D observation of defects, the welded specimens were examined under an XCT machine (GE-Phoenix® model: V/TOME/XS). For such analysis, coupons having dimensions of 10×5×3 mm^3 were cut in such a way so that the entire weldment region is covered. The parameter used for XCT scans is given in **Table–2**. Before XCT analysis, the samples were fine polished and thoroughly cleaned with acetone. For quantitative analysis such as for determination of size and number of pores, the XCT data were analyzed using the Phoenix-

Datox® (model: VG-STUDIO-MAX 2.2) software package. It is to be noted that the XCT machine used for the present investigation has a limitation for voxel size up to 10µm only. During XCT scan, to reduce ring effect, ROI CT filter was used while for maintaining the histogram ratio between the material and background, an external filter (0.5mm Cu) was used. Beam Hardening Correction **(BHC)** filter was used for reducing the artefacts and noise in final data in order to obtain clear images. For solving the fixation problem (as sample may tilt/shift while rotating during scanning) 'agc' corrections were made for scan optimization.

Table–2: XCT scanning parameters used in this study

Voltage (kV)	110	**Number of projections**	1000
Current (µA)	95	**Optical magnification**	19×
Exposure (ms)	1000	**Voxel size (µm)**	10
Filter (Cu) in mm	0.5		

3. RESULTS AND DISCUSSION

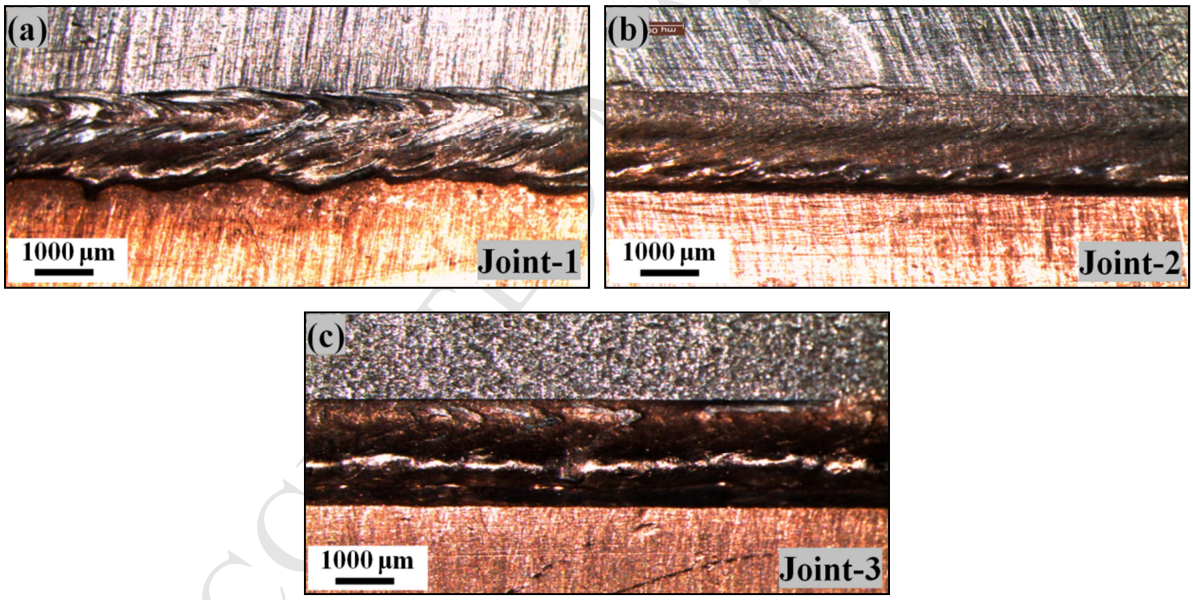

Fig. 3: Macroscopic images showing weld beads (face side) for: **(a)** joint–1, **(b)** joint–2, and **(c)** joint–3

Figure 3 represents the macroscopic images showing the weld bead surface for the three dissimilar copper–SS joints. As shown in **Fig 3(a)**, it is well revealed that the appearance of weld bead surface in joint–1 produced with non-oscillating beam is found to be quite rough; while the weld bead surfaces of joint–2 and 3 produced using oscillating beam is quite smooth as shown in **Fig 3(b)** and **Fig 3(c)**, respectively. Under non-oscillating beam

condition, spatter formation occurred when the welding speed is quite high. Oscillating beam produces an intense churning action in the weld pool which helps in producing a smooth and homogenous weld bead. This indicates that the application of beam oscillations could be used as an effective tool in reducing spatter formation in high energy density EBW processes.

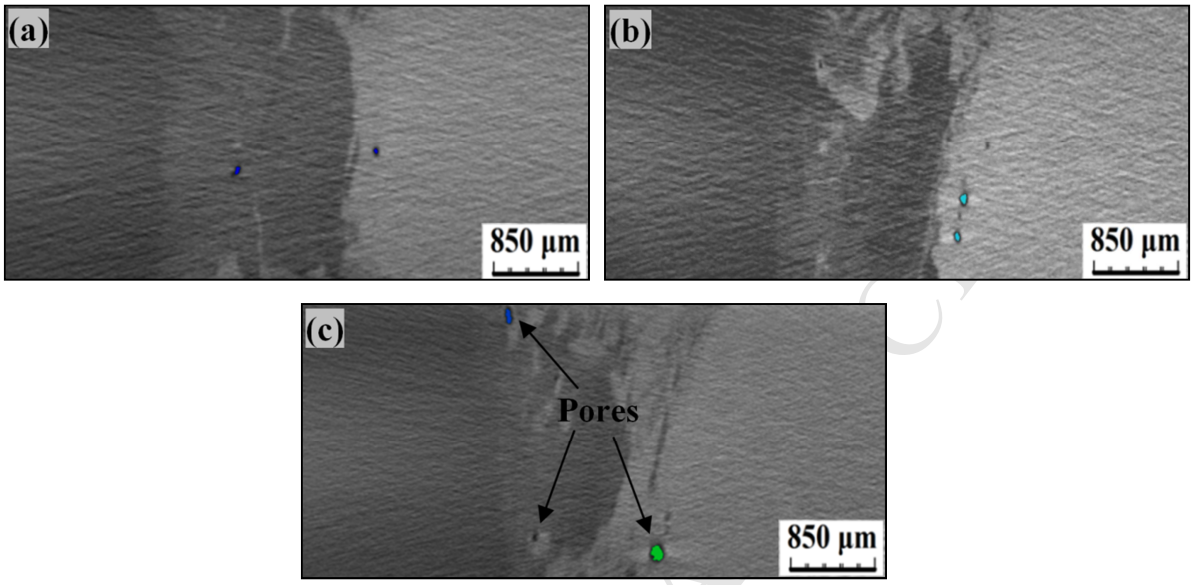

Fig. 4: Reconstructed 2D images along transverse section for: **(a)** joint–1, **(b)** joint–2, and **(c)** joint–3

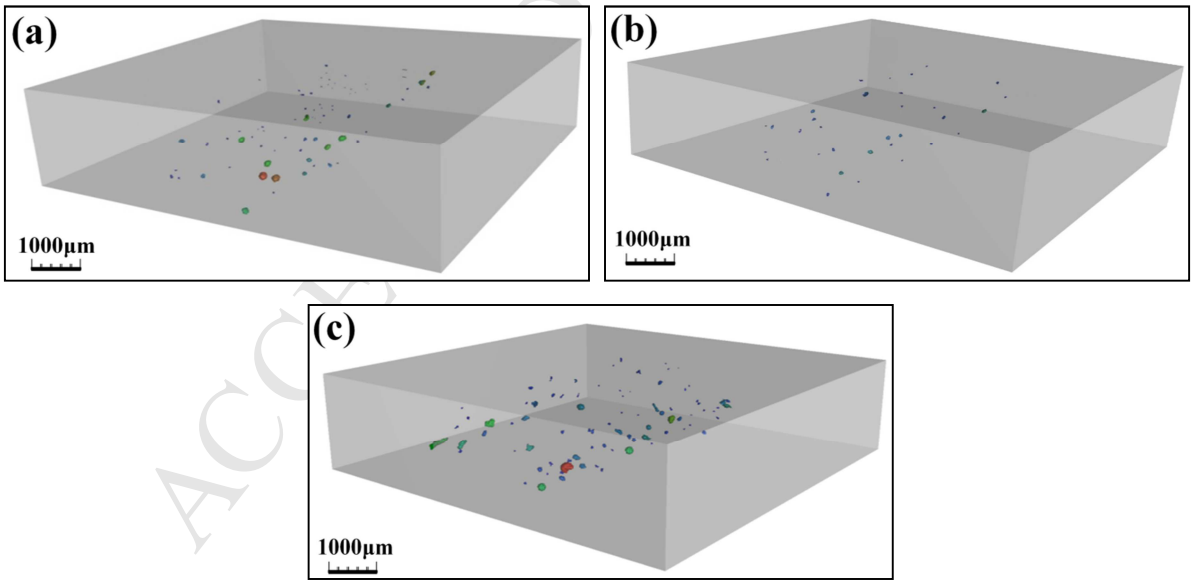

Fig. 5: Reconstructed 3D transparent images for: **(a)** joint–1, **(b)** joint–2, and **(c)** joint–3

Figure 4 shows the two-dimensional **(2D)** XCT images obtained along the transverse sections of three prepared copper–SS joints. As shown in **Fig. 4**, the darker and lighter regions represent the SS and copper side of the joint, respectively. It is to be noted that the

presence of porosity was found to be higher either in the copper rich side or in the segregated regions of unmixed copper chunks that are present in the fusion zone. **Figure 5** represents the reconstructed 3D transparent images showing porosity distribution across the fusion zone region. For better visualization, 3D reconstructed images of three joints along transverse and longitudinal sections are presented in **Fig. 6** and **Fig. 7**, respectively. Similar to **Fig. 4**, in these figures also the left side is copper side while right side is the SS side. Careful observation of **Fig. 6** and **Fig. 7** confirms that the pores are individual and are not connected to each other. For each joint, the corresponding pore numbers were counted and it was observed thatjoint–3 prepared using oscillating beam with 2mm oscillation diameter contained highest number of pores (167nos) followed by joint–1 (115nos) prepared with non-oscillating beam. The lowest number of pores (64nos) was found to be in joint–2 prepared using oscillating beam with lower oscillation diameter of 1mm.The average pore diameter for each joint has also been measured, and it was found that the joint–3 possessed coarser pores having largest pore with diameter of 201µm and smallest pore with diameter of 30µm followed by joint–1 (176µm and 16µm, respectively).Out of the three joints, joint–2 had shown the best results with largest and smallest pores having diameter of 121µm and 11µm, respectively.

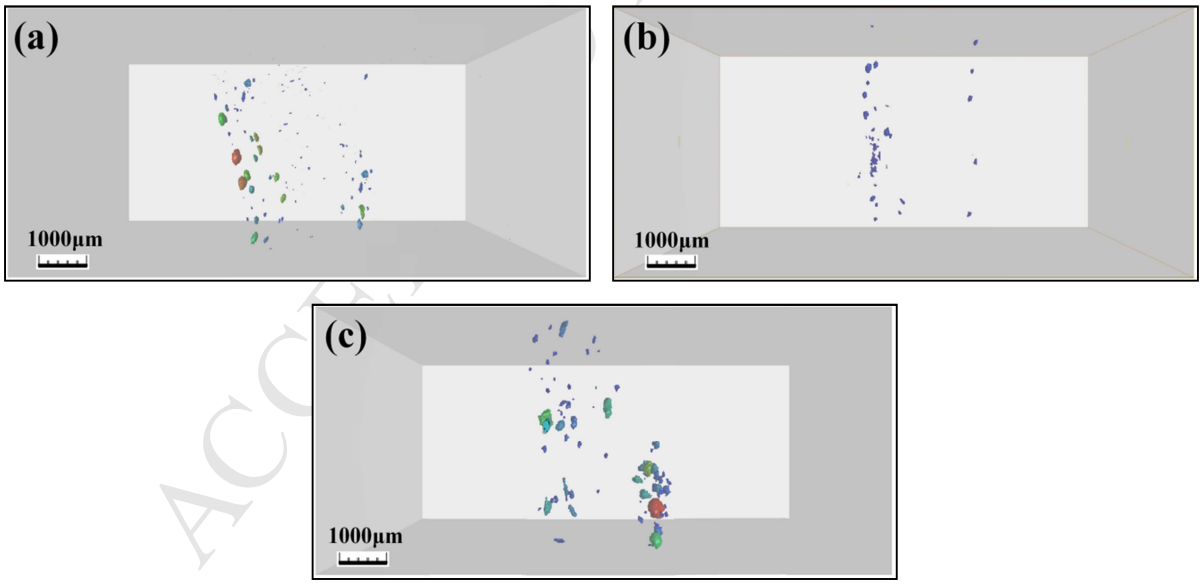

Fig. 6: Reconstructed 3D transparent images along transverse section for: **(a)** joint–1, **(b)** joint–2, and **(c)** joint–3

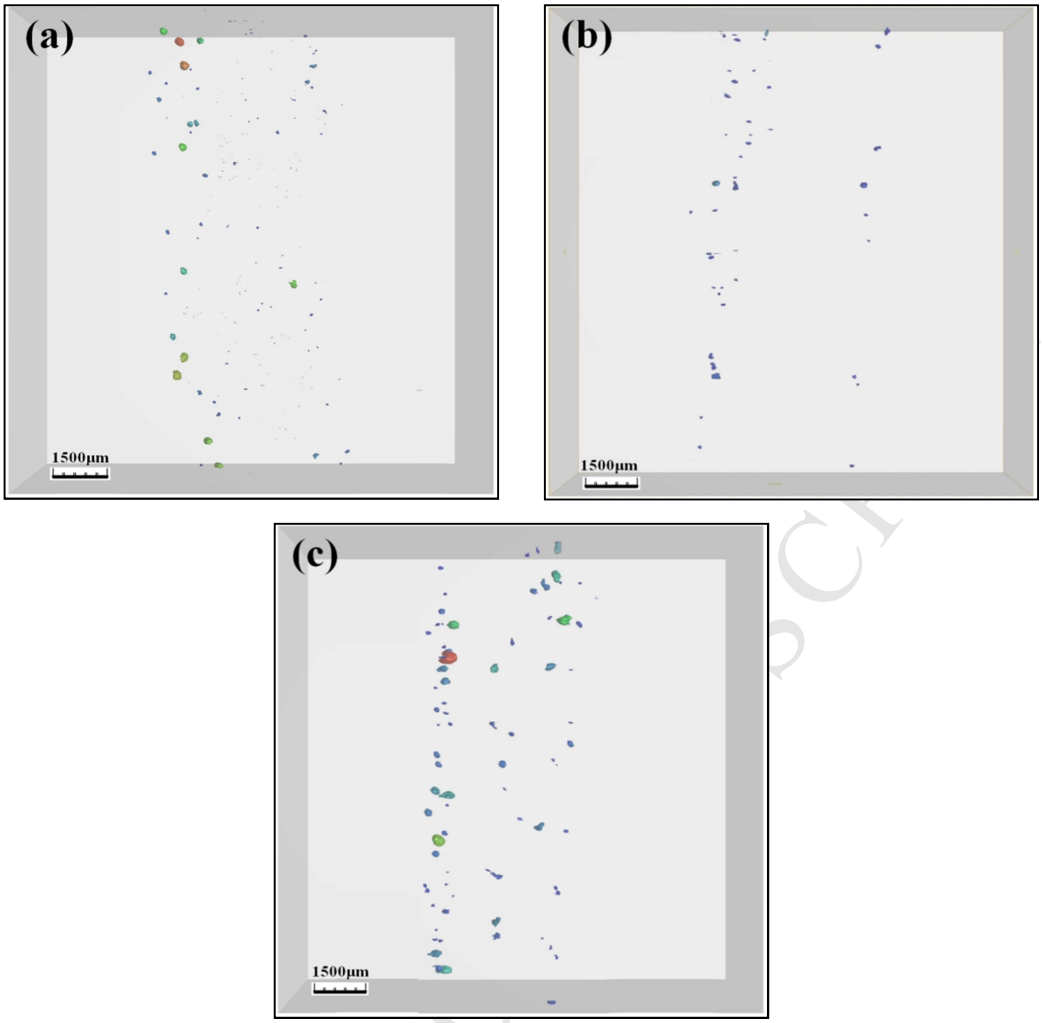

Fig. 7: Reconstructed 3D transparent images along longitudinal section for: **(a)** joint–1, **(b)** joint–2, and **(c)** joint–3

The morphology of each pore was characterized using a sphericity calculation as given in **equation–1 [23]**. For such calculations, pores having diameter below 10µm were excluded to avoid uncertainty in estimating their actual surface area.

$$\psi = \left(\frac{36\pi V_P^2}{A_P^3} \right)^{\frac{1}{3}} \quad \textbf{(1)}$$

Where, Ψ is the sphericity of pore, V_P is the volume and A_P is the surface area of the corresponding pore for a condition, where Ψ=1 represents a perfect sphere. The calculated sphericity values as a function of pore size are shown in **Fig. 8(a)**. The results shows that the majority of pores were close to spherical in shape as their sphericity values are above 0.50. It is also clear from **Fig 8(a)** that the smaller pores were having higher sphericity values than the larger pores. **Figure 8(b)** shows the 3D view of a single pore in the weld joint. As shown

in **Fig. 8(b)**, the pore is found to be in spherical shape with an irregular outer surface. From the XCT results it has been observed that the surface irregularities increased with increase in pore size as also shown in **Fig. 8(a)**.

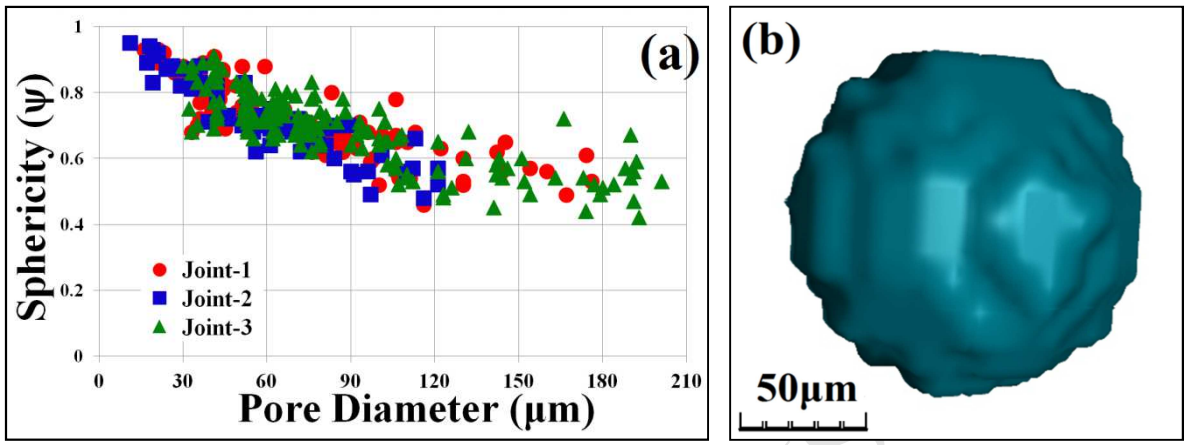

Fig. 8: (a) variation of sphericity with pore diameter, and **(b)** 3D morphology of a single individual pore in the joint–3

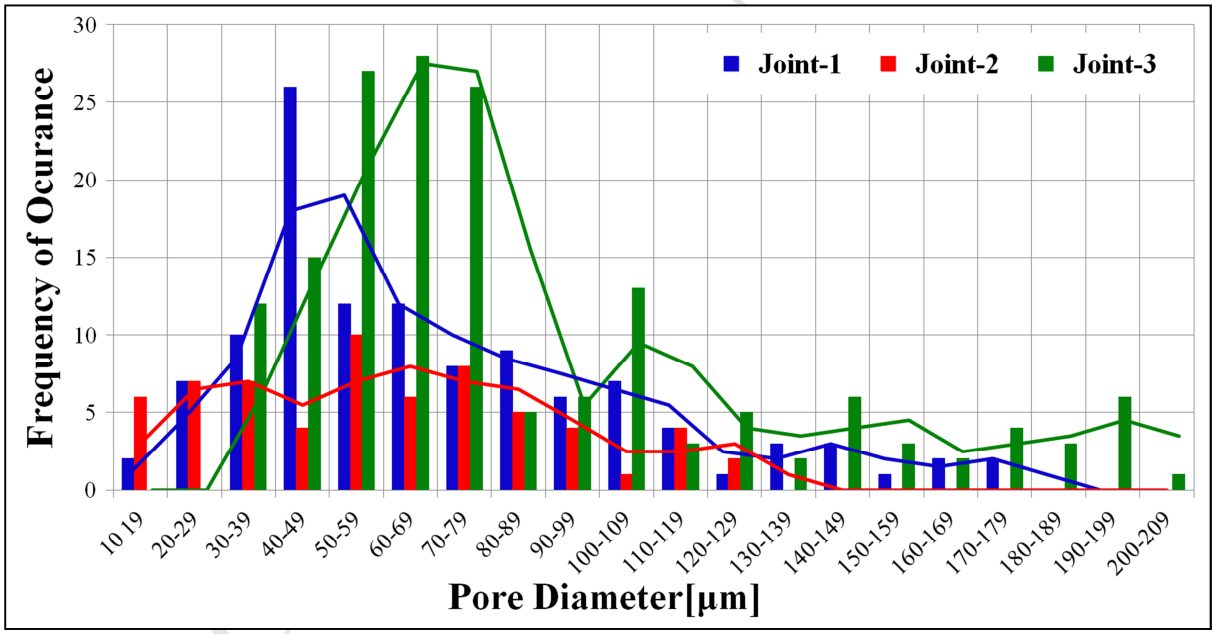

Fig. 9: Bar Diagram Showing pore size and their corresponding frequency of occurrence for the three joints

Fig. 9 depicts the frequency of occurrence for pores of different sizes for all three joints. It is seen that for all three joints irrespective of the welding conditions, majority of pores (40-50%) were in the size range of 50 to 100μm. However, some differences were observed in percentage of pores having diameter below 50μm and above 100μm for the three joints. It is observed that joint–3 contained minimum share (15%) of pores having a diameter

below 50µm followed by joint–2 (32%) while joint–1 had the maximum share of 41%. On the other hand, joint–2 contained minimum share of (11%) of pores having diameter above 100µm followed by joint–1 (20%), while joint–3 had the maximum share of 30%. **Figure 10** shows the SEM image of joint–3 showing porosity in fusion zone. In all welded joints, irrespective of the welding conditions, majority of pores were observed either near the copper side or wherever copper chunks or globules were present in the fusion zone as shown in **Fig. 10**.

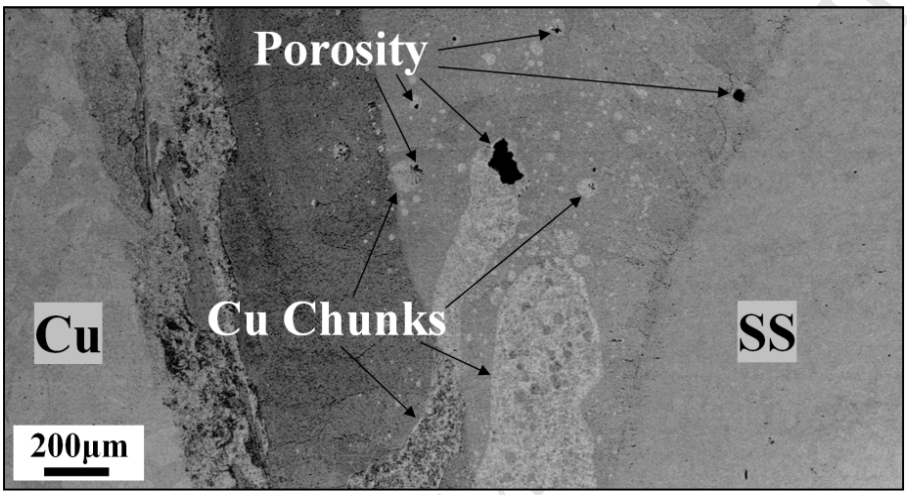

Fig. 10: FE-SEM **(BSE)** image showing porosities in the fusion zone of joint–3

4. DISCUSSION

In general, porosity formation in EBW dissimilar joints results from either (a) key-hole instabilities in the fusion zone; or (b) from volatile elements such as Zn and Mg present in the base metal; or (c) due to dissolved gasses like H and O present in the base metal; or (d) due to formation of shrinkage cavities during solidification of the weld zone. In this study, keyhole instability can be ruled out as the welding was carried out with full penetration butt-joint. Also, there was no presence of volatiles in the sample. Shrinkage cavities are unlikely to be spherical. Therefore, the only possible reason for the formation of porosity is due to nucleation of bubbles by dissolved gases on the heterogeneous sites in the welded joints. Since copper contains dissolved gases such as O and H; these gases could be the reason for formation of porosities in the joints. Moreover, it has also been clearly observed in **Fig. 4** and **Fig. 10** that the majority of pores were confined either near the copper rich side or wherever there are chunks of copper present in the fusion zone.

In case of joint–2 that is produced with beam oscillation with optimum oscillation diameter, pores and copper is more uniformly distributed in the weld; however, joint–3 that was also produced by beam oscillation but with larger oscillation diameter showed chunks of copper in the weld with larger and higher amount of pores. Thus, churning action of beam oscillation only becomes fruitful for an optimum and smaller oscillation diameter. It may be reasoned like this. With optimum oscillation diameter, beam dwelling on copper becomes marginal that melts smaller amount of copper. Such limited amount of copper is expected to go into iron solution completely and get distributed in the fusion zone by the intense churning action of weld track under beam oscillation. Subsequently, copper get separated during solidification in the form of well distributed fine droplets of copper. Since pores mostly appear in the copper because of dissolved gas in copper, beam oscillation resulted in entrapment well distributed finer pores in joint–2; But, in case of joint–3, produced with beam oscillation but with larger oscillation diameter, beam dwells on copper for larger amount of time and melts larger amount of copper. Such larger amount of copper might not dissolve in iron and may not utilize the churning action of beam oscillation for its distribution being dissolved in the major phase iron. This might result in segregated mass of copper in the form of chunks in the solidified weld track. Such improper distribution of copper leads to larger and more pores in the in joint–3. Another phenomenon that influences pore entrapment is repeated melting of the same spot that allows releasing gases during subsequent melting **[29]**. It has been hypothesized that high energy density EBW can be conceived as melting of numerous tiny weld pools in succession with significant overlapping between them. Such overlapping becomes more intense and complicated in case of beam oscillation **[32-34]**. Such intense overlapping of pools allows repeated melting of the same spot and may release gas pores resulting in less and uniformly distributed pores in weld joints as shown in joint–2. Although joint–3 was also produced by beam oscillation, the reduction in gases by repeated melting of the same spot was less than compensated by that due to segregated volume of gas in the copper chunks in the weld track. In case of joint–1, produced without beam oscillation, melt mixing was poor and spot overlapping and re-melting was also less intense that might lead to a large number of entrapped pores of different sizes.

5. CONCLUSIONS

- It was observed that the application of beam oscillation reduced the pore size and its content in the joint compared to that produced by their non-oscillating counterpart. It

was further observed that porosity size and amount increased with increase in oscillation diameter beyond an optimum diameter. Beam oscillation produces heat and mass mixing in the weld track by intense and complex overlapping of tiny weld pools formed in succession along its trajectory. Besides, repeated melting of the same spot due to complex spot overlapping between two successive weld pools also releases the entrapped gas. Therefore, beam oscillation reduces both size and amount of pores. However, beam with higher oscillation diameter melts larger amount of copper that may not dissolve in iron for subsequent mixing in the weld track. Thus copper remains as segregated mass with larger pores.

- In all joints, it was observed that the fine pores were formed in steel matrix, while coarse and large pores were formed in copper matrix, which may be attributed to the fact that copper contained more dissolved gases than iron.

ACKNOWLEDGEMENT: The authors gratefully acknowledge the financial help received from the Board of Research for Nuclear Science, Department of Atomic Energy, Government of India.

REFERENCES

[1] Z. Sun, and J.C. Ion, Review-Laser welding of dissimilar metal combinations, **J. Mater. Sci.**, 30, (1995), 4205–4214.

[2] Z. Sun, and R. Karppi, The application of electron beam welding for the joining of dissimilar metals: an overview, **J. Mater. Process. Technol.**, 59, (1996), 257–267.

[3] O. Yilmaz, and M. Aksoy, Investigation of micro-crack occurrence conditions in diffusion bonded Cu-304 stainless steel couple, **J. Mater. Process. Technol.**, 121, (2002), 136–142.

[4] A. Durgutlu, B. Gulenc¸, and F. Findik, Examination of copper / stainless steel joints formed by explosive welding, **Mater. Des.**, 26, (2005) 497–507.

[5] H. Sabetghadam, A.Z. Hanzaki, A. Araee, and A. Hadian, Microstructural evaluation of 410 SS / Cu diffusion-bonded joint, **J. Mater. Sci. Technol.**, 26(2), (2010), 163–169.

[6] Y. Imani, M.K. Besharati and M. Guillot, Improving friction stir welding between copper and 304L stainless steel, **Adv. Mater. Res.**, 409, (2012), 263–268.

[7] J. Xiong, Q. Xie, J. Li, F. Zhang, and W. Huang, Diffusion bonding of stainless steel to copper with tin bronze and gold interlayers, **J. Mater. Eng. Perform.**, 21(1), (2012), 33–37.

[8] C. Shanjeevi, S.S. Kumar, and P. Sathiya, Multi-objective optimization of friction welding parameters in AISI 304Laustenitic stainless steel and copper joints, **Proc. I Mech E Part B: J Eng. Manuf.**, 230(3), (2016), 449–457.

[9] S.G. Shiri, M. Nazarzadeh, M. Sharifitabar, and M.S. Afarani, Gas tungsten arc welding of CP-copper to 304 stainless steel using different filler materials, **Trans. Nonferrous Met. Soc. China**, 22, (2012), 2937–2942.

[10] M. Velu, and S. Bhat, Metallurgical and mechanical examinations of steel–copper joints arc welded using bronze and nickel-base superalloy filler materials, **Mater. Des.**, 47, (2013), 793–809.

[11] C. Roy, V.V. Pavanam, G. Vishnu, P.R. Hari, M. Arivarasu, M. Manikandam, D. Rajkumar, and N. Arivazhagan, Characterization of metallurgical and mechanical properties of commercially pure copper and 304 dissimilar weldments, **Proc. Mater. Sci.**, 5, (2014), 2503–2512.

[12] Y. Zhang, J. Huang, H. Chi, N. Cheng, Z. Cheng, and S. Chen, Study on welding – brazing of copper and stainless steel using tungsten / metal gas suspended arc welding, **Mater. Lett.**, 156, (2015), 7–9.

[13] C. Yao, B. Xu, X. Zhang, J. Huang, J. Fu, and Y. Wu, Interface microstructure and mechanical properties of laser welding copper – steel dissimilar joint, **Opt. Las. Eng.**, vol. 47, (2009), 807–814.

[14] S. Chen, J. Huang, J. Xia, H. Zhang, and X. Zhao, Microstructural characteristics of a stainless steel/copper dissimilar joint made by laser welding, **Metall. Mater. Trans. A**, 44(8), (2013), 3690–3696.

[15] S.V. Kuryntsev, A.E. Morushkin, and A.K. Gilmutdinov, Fiber laser welding of austenitic steel and commercially pure copper butt joint, **Opt. Las. Eng.**, 90, (2017), 101–109

[16] T. Wang, Y. Zhang, X. Li, B. Zhang, and J. Feng, Influence of beam current on microstructures and mechanical properties of electron beam welding-brazed aluminum-steel joints with an Al5Si filler wire, **Vacuum**, (2017), 281–287

[17] A. Hajitabar, and H.N. Moosavy, Electron beam welding of difficult-to-weld austenitic stainless steel/Nb-based alloy dissimilar joints without interlayer, **Vacuum**, 146, (2017), 170–178

[18] W. Ting, Z. Bing-gang, and C. Guo-qing, Electron beam welding of Ti-15-3 titanium alloy to 304 stainless steel with copper interlayer sheet, **Trans. Nonferrous Met. Soc. China**, 20(10), (2010), 1829–1834.

[19] T.K. Saha, A.K. Ray, B.K. Shah, K. Bhanumurthy, and G. Kale, Electron beam welding of copper to AISI-304 SS, **Inter. Weld. Conf.–IWC'99**, New Delhi, India, (1999), 63–71.

[20] S. Guo, Q. Zhou, J. Kong, Y. Peng, Y. Xiang, and T. Luo, Effect of beam offset on the characteristics of copper / 304stainless steel electron beam welding, **Vaccum**, 128, (2016), 205–212.

[21] I. Magnabosco, P. Ferro, F. Bonollo, and L. Arnberg, An investigation of fusion zone microstructures in electron beam welding of copper–stainless steel, **Mater. Sci. Engineer. A**, 424, (2006), 163–173.

[22] S.G. Wang, X.H. Ji, X.Q. Zhao, and N.N. Dong, Interfacial characteristics of electron beam welding joints of SiCp/Al composites, **Mater. Sci. Technol.**, 27(1), (2011),60–64.

[23] S.K. Dinda, J.M. Warnett, M.A. Williams, G.G. Roy, and P. Srirangam, 3D imaging and quantification of porosity in electron beam welded dissimilar steel to Fe-Al alloy joints by X-ray tomography, **Mater. Des.**, 96, (2016), 224–231.

[24] M. Kraetzsch, J. Standfuss, A. Klotzbach, J. Kaspar, B. Brenner, and E. Beyer, Laser beam welding with high-frequency beam oscillation: welding of dissimilar materials with brilliant fiber lasers, **Phys. Proceed.**, 12, (2011), 142–149.

[25] P. Fu, Z. Mao, Y. Wang, Z. Tang, and C. Zuo, Fatigue properties of heavy-thickness Ti6.5Al2Zr1Mo1V alloy with oscillation EBW, **Vacuum,** 121, (2015), 230–235.

[26] L. Wang, M. Gao, C. Zhang, and X. Zeng, Effect of beam oscillating pattern on weld characterization of laser welding of AA6061-T6 aluminum alloy, **Mater. Des.,** 108, (2016), 707–717

[27] J.L. Huang, N. Warnken, J.C. Gebelin, M. Strangwood, and R.C. Reed, On the mechanism of porosity formation during welding of titanium alloys, **Acta Mater.,** 60, (2012), 3215–3225.

[28] T. Mohandas, D. Banerjee, and V.V.K. Rao, Fusion zone microstructure and porosity in electron beam welds of an α+β titanium alloy, **Metall. Mater. Trans. A,** 1999, vol. 30A, pp. 789–798

[29] X.L. Gao, L.J. Zhang, J.Liu, and J.X. Zhang, Porosity and microstructure in pulsed Nd:YAG laser welded Ti6Al4V sheet, **J. Mater. Process. Technol.,** 2014, vol. 214, pp. 1316–1325.

[30] C. Wiednig, F. Stiefler, and N. Enzinger, Influence of surface roughness in electron beam welding, **IOP Conf. Series: Mater. Sci. Eng.,** 2016, vol. 119, pp. 1–8.

[31] V.V. Redchits, Scientific fundamentals and measures used to prevent the formation of pores in fusion welded titanium and its alloys, **Weld. Intern.,** 1997, vol. 1(9), pp. 722–728.

[32] J. Kar, S.K. Roy, and G.G. Roy, Effect of beam oscillation on electron beam welding of copper with AISI-304 stainless steel, **J. Mater. Process. Technol.,** 2016, vol. 233, pp. 174–185.

[33] J. Kar, S.K. Roy, and G.G. Roy, Effect of beam oscillation on electron beam welding of copper with AISI-304 stainless steel, **Metall. Mater. Trans. A**, 48(4), (2017), 1759–1770.

[34] J. Kar, S.K. Roy, and G.G. Roy, Influence of beam oscillation in electron beam welding of Ti–6Al–4V, **Int. J. Adv. Manuf. Technol.**, 93(5-8), (2017), 1–11.

Figure Caption

Fig. 1	80 kV, 12 kW Electron Beam Welding **(EBW)** machine at IIT Kharagpur
Fig. 2	X-ray radiographic images of the three prepared copper–SS joints
Fig. 3	Macroscopic images showing weld beads (face side) for: **(a)** joint–1, **(b)** joint–2, and **(c)** joint–3
Fig. 4	Reconstructed 2D images along transverse section for: **(a)** joint–1, **(b)** joint–2, and **(c)** joint–3
Fig. 5	Reconstructed 3D transparent images for: **(a)** joint–1, **(b)** joint–2, and **(c)** joint–3
Fig. 6	Reconstructed 3D transparent images along transverse section for: **(a)** joint–1, **(b)** joint–2, and **(c)** joint–3
Fig. 7	Reconstructed 3D transparent images along longitudinal section for: **(a)** joint–1, **(b)** joint–2, and **(c)** joint–3
Fig. 8	**(a)** variation of sphericity with pore diameter and **(b)** 3D morphology of a single individual pore in the joint–3
Fig. 9	Bar Diagram Showing pore size and their corresponding frequency of occurrence for the three joints
Fig. 10	FE-SEM **(BSE)** image showing porosities in the fusion zone of joint–3

Table Caption

Table–1	Chemical composition of 304 SS and copper (C10300) in weight percentage
Table–2	XCT scanning parameters used in this study

The problem of porosity formation in similar and dissimilar metals/alloys joints, produced by high energy density heat source like laser and electron beam are well known. The effect of electron beam oscillation that produces a churning action in the liquid weld pool is supposed to homogenize the liquid and reduce the amount and size of entrapped gas bubbles, or porosity. The present article, for the first time an attempt has been made to study the effect of beam oscillation on porosity in copper - stainless steel (SS) dissimilar joints.

The highlights of the present study are as follows:

- Copper to 304SS sheets having a thickness of 3mm were successfully joined by electron beam welding process using both oscillating and non-oscillating beam.
- The porosity content in the weld zone of the prepared joints are investigated by using X-ray computed tomography (XCT) technique.
- It has been found that under an oscillating beam with lower oscillation diameter, the size and number of pores in the weld zone decrease significantly.
- Moderate copper melting and its mixing in the fusion zone under oscillating beam of lower oscillation diameter has resulted lower porosity formation.
- The pore numbers were found to be higher for non-oscillating beam or oscillating beam with higher oscillation diameter.
-